in LB films. The inability of the four-point probe to penetrate 3 layers of QDP on InSnO is also a tribute to the hardness and coherence of the multilayer. This manifestation of insulating ability parallels the previously reported electrochemical passivation of a gold electrode by an aliphatic zirconium diphosphonate monolayer.[12b]

Future goals of this effort are to exploit both the strength and electronic properties of multilayers prepared by self-assembly. The relative unresponsiveness of such films to chemical, mechanical, and thermal stress point to possible uses in insulation and passivation. We would also like to incorporate this general robustness into films that are more electronically active as a whole. Replacement of the nonoxidizable and nonreducible zirconium phosphonate interlayer with an interlayer that could act as an electron donor or acceptor in its own right is one strategy under consideration for the design of multilayers in which interlayer electron transfer could be observed. The quaterthiophene building block, because of its oxidizability and demonstrated suitability for packing in multilayers, may be appropriate for electroactive multilayered materials.

Acknowledgment. We are grateful to R. C. Haddon for advice and assistance with the electrical measurements and to L. Brus for helpful discussions.

Ionic Conductivities of Ion-Exchanged $A_3Sb_3P_2O_{14}$ (A = Na, K, Rb), $A_5Sb_5P_2O_{20}$ (A = Li, Na, K, Rb), and Partially Substituted $K_5Sb_{5-x}M_xP_2O_{20}$ (M = Nb, Ta)

E. Wang and M. Greenblatt*

Department of Chemistry, Rutgers, The State University of New Jersey, Piscataway, New Jersey 08854

Received March 21, 1990. Revised Manuscript Received May 13, 1991

The ionic conductivities of ion-exchanged compounds were measured in $A_3Sb_3P_2O_{14}$ (A = Na, K, Rb) and $A_5Sb_5P_2O_{20}$ (A = Li, Na, K, Rb) with two-dimensional (2D) layered and three-dimensional (3D) framework structures, respectively. In layered $A_3Sb_3P_2O_{14}$, the mobility of the cations alone determine the ionic conductivity. In $A_5Sb_5P_2O_{20}$ with framework structure, both the bottleneck size and the mobility of the cations affect the observed ionic conductivity. Partial replacement of Sb by Ta/Nb in the highest conducting $K_5Sb_5P_2O_{20}$ sample lead to improvement of the ionic conductivity by 1 order of magnitude ($\sim 10^{-3}$ $(\Omega\ cm)^{-1}$ at 500 °C) in $K_5Sb_3Nb_2P_2O_{20}$. The optimal bottleneck size appears to be in $K_5Sb_3Nb_2P_2O_{20}$, since no further improvement in the ionic conductivity is observed in $K_5Sb_2Ta_3P_2O_{20}$, which has a larger bottleneck than $K_5Sb_3Nb_2P_2O_{20}$.

Introduction

Piffard et al.[1-5] recently reported a series of potassium phosphatoantimonates (K–Sb–P–O), hereafter KPA) with structures ranging from quasi-one-dimensional (1D) to quasi-two-dimensional (2D) to three-dimensional (3D) network. Among these KPAs, the $K_nSb_nP_2O_{3n+5}\cdot xH_2O$ (n = 1, 3, 5) series[6-8] has been found to exhibit good ion-exchange properties. During our recent study[9] on the ionic conductivity of these KPAs, we found that the n = 5 member of the series, $K_5Sb_5P_2O_{20}$, has the highest ionic conductivity ($\sim 10^{-3}$ $(\Omega\ cm)^{-1}$ at 500 °C) of all the KPAs investigated. This was attributed to its skeleton structure (Figure 1) with interconnected, large and mostly vacant tunnels that facilitate the motion of K^+ ions. The ionic conductivity of this phase was improved by an order of magnitude when potassium was ion-exchanged by sodium. In this work we investigated the effects of various substitutions on the ionic conductivity of $K_5Sb_5P_2O_{20}$, which includes the isomorphous replacement of Sb^{5+} by V^{5+}, Nb^{5+}, or Ta^{5+} and partial replacement of P^{5+} by Si^{4+}. The former should affect the size of the bottleneck only while the latter will also require an increase in the K^+ content to maintain charge neutrality. Finally, we carried out detailed ion-exchange studies on the 3D $K_5Sb_5P_2O_{20}$ and the layered $K_3Sb_3P_2O_{14}$ in order to compare the ease of ion-exchange with structural dimensionality and the resultant ionic conductivities. These results are presented in this paper.

Experimental Section

$K_3Sb_3P_2O_{14}$ and $K_5Sb_5P_2O_{20}$ were prepared as described previously.[4,5] Partial substitutional reactions were carried out by replacing some of the P_2O_5 by SiO_2 in $K_{5+x}Sb_5P_{2-x}Si_xO_{20}$ and some of the Sb_2O_3 by $V_2O_5/Nb_2O_5/Ta_2O_5$ (all chemicals were at least reagent grade purity) in $K_5Sb_{5-x}M_xP_2O_{20}$ (M = V, Nb, Ta). The reaction temperature varied according to the nature of the substituent: 1000 °C for $K_5Sb_{5-x}V_xP_2O_{20}$, 1070 °C for $K_5Sb_{5-x}Nb_xP_2O_{20}$, and 1100 °C for $K_5Sb_{5-x}Ta_xP_2O_{20}$. Higher reaction temperatures led to melting in the case of vanadium- and niobium-substituted KPAs.

Ion-exchange reactions were carried out via hydrothermal autoclave synthesis, by the molten salt method, or indirectly by the ion-exchange of the protonated phosphatoantimonates.

(1) Lachgar, A.; Deniard-Courant, S.; Piffard, Y. *J. Solid State Chem.* **1986**, *63*, 409.
(2) Piffard, Y.; Oyetola, S.; Courant, S.; Lachgar, A. *J. Solid State Chem.* **1985**, *60*, 209.
(3) Piffard, Y.; Lachgar, A.; Tournoux, M. *J. Solid State Chem.* **1985**, *58*, 253.
(4) Piffard, Y.; Lachgar, A.; Tournoux, M. *Mater. Res. Bull.* **1986**, *21*, 1231.
(5) Piffard, Y.; Lachgar, A.; Tournoux, M. *Mater. Res. Bull.* **1985**, *20*, 715.
(6) Piffard, Y.; Verbaere, A.; Oyetola, S.; Deniard-Courant, S.; Tournoux, M. *Eur. J. Solid State Inorg. Chem.* **1989**, *26*, 113.
(7) Piffard, Y.; Verbaere, A.; Lachgar, A.; Deniard-Courant, S.; Tournoux, M. *Rev. Chim. Miner.* **1986**, *23*, 766.
(8) Tournoux, M.; Piffard, Y. French Patent 85-10839.
(9) Wang, E.; Greenblatt, M. *Chem. Mater.* in press.

0897-4756/91/2803-0703$02.50/0

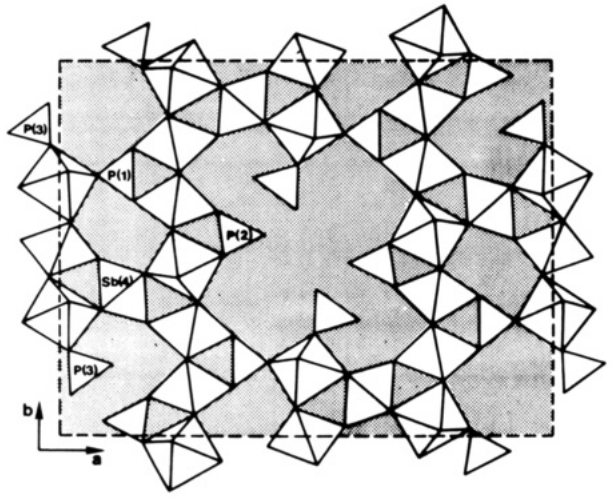

Figure 1. [001] view of the ($Sb_5P_2O_{20}^{5-}$) framework.[4]

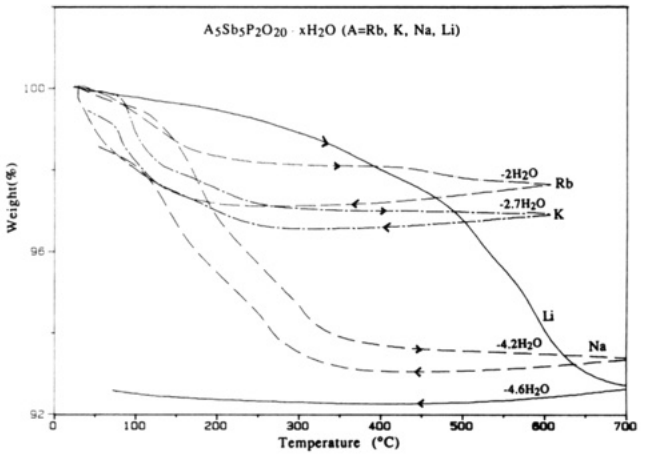

Figure 2. TGA of $A_5Sb_5P_2O_{20}{\cdot}xH_2O$ (A = Rb, K, Na, Li).

Details of these techniques were described in a previous paper.[9] The resulting compounds were analyzed by powder X-ray diffraction (Scintag PAD V). Ionic conductivity measurements were carried out by an ac complex imepdance technique using a Solartron 1250 frequency analyzer and a 1186 electrochemical interface. Data collection and analysis were done with a Hewlett-Packard 9816 desktop computer. Samples were pelletized and sintered at 700 °C for a few hours before coating the surfaces of the pellets with platinum paste. A frequency range of 10 Hz to 65 kHz was employed at a heating rate of 3 °C/min from 200 to 650 °C in flowing helium. Weight loss due to water in the samples was monitored in an automated DuPont 950 thermogravimetric analyzer (TGA). Chemical analysis was performed with a Beckman plasma spectrometer.

Results and Discussions

Ion-Exchanged Phosphatoantimonates. Successful ion-exchange reactions were observed in $K_5Sb_5P_2O_{20}$ with Li, Na, and Rb replacing K. $Li_5Sb_5P_2O_{20}$ was obtained from a molten solution of $LiNO_3$. $Na_5Sb_5P_2O_{20}$ was obtained hydrothermally from a 1 M $NaNO_3$ aqueous solution, and $Rb_5Sb_5P_2O_{20}$ was prepared indirectly via the reaction of $H_5Sb_5P_2O_{20}$ and RbOH. TGA measurements show that the ion-exchanged compounds are hydrated (Figure 2). The amounts of hydrate water in the phosphatoantimonates increase with decreasing size of the alkali-metal ions: $Li_5Sb_5P_2O_{20}{\cdot}4.6H_2O$, $Na_5Sb_5P_2O_{20}{\cdot}4.2H_2O$, $K_5Sb_5P_2O_{20}{\cdot}2.7H_2O$, and $Rb_5Sb_5P_2O_{20}{\cdot}2H_2O$. The temperatures at which a steady state (i.e., constant weight) is reached in the TGA curves decrease from ~700 °C in $Li_5Sb_5P_2O_{20}$ to ~200 °C in $Rb_5Sb_5P_2O_{20}$. The TGA curves indicate a reversible behavior of water loss/gain for the

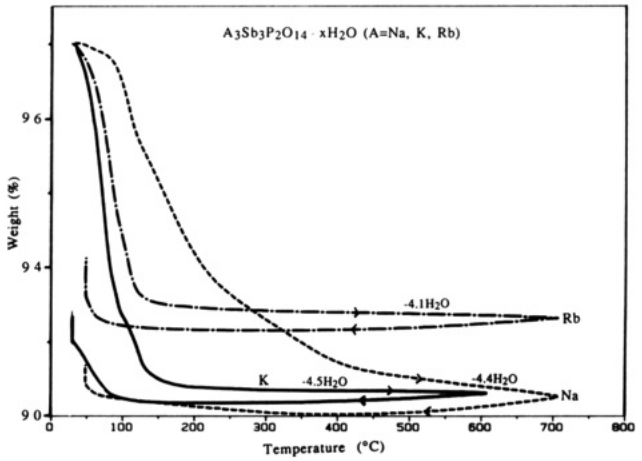

Figure 3. TGA of $A_3Sb_3P_2O_{14}{\cdot}xH_2O$ (A = Na, K, Rb).

rubidium, potassium, and sodium phosphatoantimonates. There are two regions of temperature where the weight loss reaches a plateau in the potassium and sodium analogues. However, $Li_5Sb_5P_2O_{20}{\cdot}4.6H_2O$ shows a steady weight loss until ~700 °C; no weight gain is seen upon cooling, which indicates irreversible behavior. These findings are consistent with the water of hydration located in the large cavities of the skeleton structure. As the size of the cation in the cavities becomes smaller (i.e., from Rb^+ to Li^+), more space is available for additional water in the cavities, leading to an increase in the amounts of hydrate water. The two plateaus seen in the TGA curves of potassium and sodium phosphatoantimonates probably correspond to water bonded at two different sites in the same cavity or in cavities of different sizes. In $Rb_5Sb_5P_2O_{20}{\cdot}2H_2O$ the large size of Rb^+ limits the location of the hydrate water to only one site. Thus, only one transition is observed at ~200 °C (Figure 2). In $Li_5Sb_5P_2O_{20}{\cdot}4.6H_2O$ a steady state was reached only above ~700 °C. The continuous loss of water in the lithium analogue indicates that large ions are needed to stabilize the large cavities. Without the hydrate water, the structure collapses as seen in the near-amorphous X-ray powder diffraction pattern of a post-TGA $Li_5Sb_5P_2O_{20}$ sample heated to 700 °C. The requirement for a large number of water molecules in the cavities to stabilize the compound probably also accounts for the decreasing trend of critical temperatures (i.e., the temperature at which the loss of water is complete) from $Li_5Sb_5P_2O_{20}$ to $Rb_5Sb_5P_2O_{20}$. A similar phenomenon was reported for ion-exchange compounds of the sodalite (a type of zeolite) series[10] in which the breakdown of the crystal structure is displaced to higher temperatures for larger cations.

For the layered $K_3Sb_3P_2O_{14}{\cdot}xH_2O$, successful ion-exchange reactions were observed when potassium was replaced by sodium or rubidium. The X-ray powder diffraction pattern of the Li analogue was not sufficiently crystalline, and hence further characterization was not carried out. Rubidium phosphatoantimonate was prepared hydrothermally from the reaction of 1 M $RbNO_3$ with $K_3Sb_3P_2O_{14}$ at 200 °C for ~15 h. Sodium phosphatoantimonate was prepared by reacting $K_3Sb_3P_2O_{14}$ in molten $NaNO_3$ at 400 °C. TGA measurements (Figure 3) on these samples indicate that they were all hydrated. However, in contrast to the ion-exchanged compounds of $K_5Sb_5P_2O_{20}$, the amounts of water hydrated are approximately the same (Figure 3) for the ion-exchanged samples as for $K_3Sb_3P_2O_{14}$. This is consistent with the hydrate water and

(10) Kelemen, G.; Lortz, W.; Schon, G. *J. Mater. Sci.* **1989**, *24*, 333.

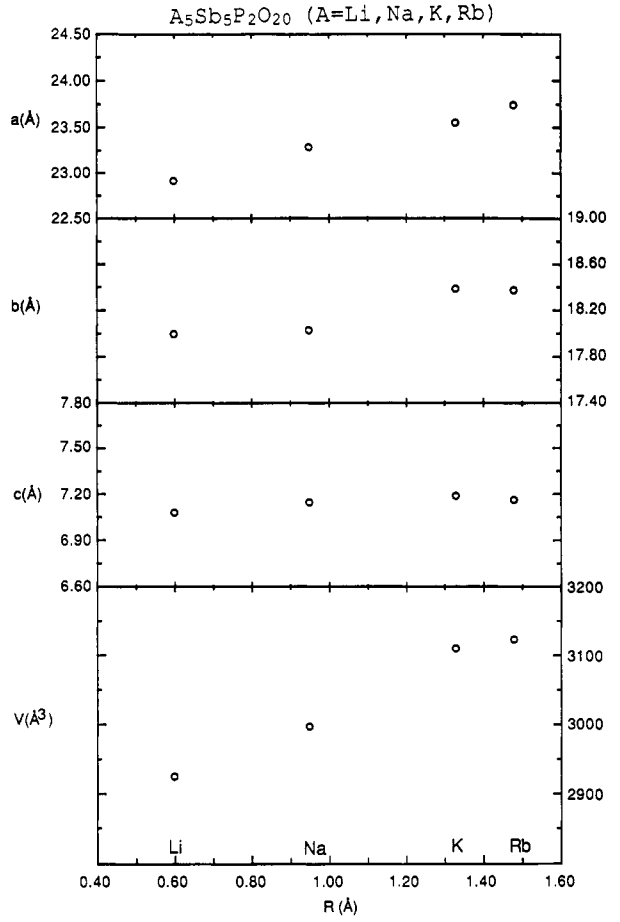

Figure 4. Variation of the unit-cell parameters as a function of the cations in $A_5Sb_5P_2O_{20}$ (A = Li, Na, K, Rb).

the cations located between the $(Sb_3P_2O_{14}^{3-})$ layers. Furthermore, since the layers are flexible (unlike the rigid framework of $K_5Sb_5P_2O_{20}$), the maximum amount of water is hydrated between the layers regardless of the size of the cation.

Least-squares-refined cell parameters of ion-exchanged $K_5Sb_5P_2O_{20}$ show an increase with increasing size of the cations (Figure 4). The increase is more pronounced in the *a* direction than along either *b* or *c*, because along *a* the SbO_6 octahedra and PO_4 tetrahydra corner-share, whereas along *b* some of the SbO_6 octahedra edge-share. Moreover, the "ringlike" feature along *c* or the "chainlike" feature along *b* (Figure 5) results in a more rigid connection than along *a*.

Next, the ionic conductivity of the aforementioned ion-exchanged samples will be discussed. In the $A_5Sb_5P_2O_{20}$ (A = Li, Na, K, Rb) series, the ionic conductivity of the Rb phosphatoantimonate is at least 1 order of magnitude lower than that of $K_5Sb_5P_2O_{20}$, and the ionic conductivity of the Na phosphatoantimonate is 1 order of magnitude higher than that of $K_5Sb_5P_2O_{20}$ (Figure 6). With the exception of Li phosphatoantimonate, the activation energies (E_a) increase with increasing size of the A cation, and there is good correlation between the conductivity and E_a (Table I). Typically, the smaller the cation, the higher the conductivity, because in general, small ions can diffuse through the bottleneck easier than big ions. The difference in mobility also contributes to the large difference seen in the ionic conductivities of Na, K, and Rb phosphatoantimonate. Nevertheless, even though Li^+ is the lightest and the smallest of the cations studied, it is also the most polarizing. This dominates the transport process in $Li_5Sb_5P_2O_{20}$, resulting in the observed high E_a

Table I. Activation Energies (E_a) of the Ion-Exchanged and Partially Substituted Potassium Phosphatoantimonates

compd	E_a, eV	compd	E_a, eV
$Li_5Sb_5P_2O_{20}$	0.623	$K_5Sb_4TaP_2O_{20}$	0.352
$Na_5Sb_5P_2O_{20}$	0.356	$K_5Sb_3Ta_2P_2O_{20}$	0.345
$K_5Sb_5P_2O_{20}$	0.519	$K_5Sb_2Ta_3P_2O_{20}$	0.247
$Rb_5Sb_5P_2O_{20}$	0.853	$K_5Sb_4NbP_2O_{20}$	0.381
$Na_3Sb_3P_2O_{14}$	0.813	$K_5Sb_3Nb_2P_2O_{20}$	0.408
$K_3Sb_3P_2O_{14}$	0.587		
$Rb_3Sb_3P_2O_{14}$	0.650		

Table II. Electronegativities and Ionic Radii of Relevant Pentavalent Ions

ion	electronegativity (χ_i)[14]	r,[13] Å
Nb^{5+}	1.6	0.78
Ta^{5+}	1.5	0.78
Sb^{5+}	2.05	0.74
V^{5+}	1.63	0.68

and the lower than expected absolute conductivity. Similar trends are seen in the Li and Na analogues of β-alumina.[11]

In $A_3Sb_3P_2O_{14}$, the $(Sb_3P_2O_{14}^{3-})$ slabs are held together by the A cations, and one expects the interlayer spacing to increase with the size of the cation. Thus, the bottleneck can vary, and the mobility of the cation is the determining factor of the magnitude of ionic conductivity. As a result, both $K_3Sb_3P_2O_{14}$ and $Rb_3Sb_3P_2O_{14}$ have similar E_a's but different preexponential terms (Figure 7). Similar results were also observed in the quasi-1D K_2SbPO_6 and Rb_2SbPO_6,[9] both of which have about the same E_a (i.e., the flexible chains can accommodate the increase in size from potassium to rubidium), but the conductivity is lower in Rb_2SbPO_6 (Rb^+ has a lower mobility than K^+). This is in contrast to the rubidium-exchanged 3D $Rb_5Sb_5P_2O_{20}$, which has a lower ionic conductivity but a higher E_a than that of $K_5Sb_5P_2O_{20}$, which indicates the inflexibility of the bottleneck in the rigid framework structure.

The ionic conductivity of $Na_3Sb_3P_2O_{14}$ is at least 1 order of magnitude higher than that of $K_3Sb_3P_2O_{14}$, even though the E_a of the Na compound is higher than that of the K analogue. This could be explained by Na^+ ions diffusing along sites in $Na_3Sb_3P_2O_{14}$ with a monoclinic symmetry, different from those of K^+ ions in $K_3Sb_3P_2O_{14}$ with rhombohedral symmetry.[7] Alternatively, the anomalously high E_a and σ in the Na phase could be attributed to a slight decomposition in $Na_3Sb_3P_2O_{14}$, which is undetected by X-ray powder diffraction. Partial decomposition could also explain the irreversibility of the heating and cooling cycles of the TGA curves in $Na_3Sb_3P_2O_{14}\cdot xH_2O$ (Figure 3).

Partially Substituted Phosphatoantimonates. Attempts were made to replace some of the phosphorus by silicon in $K_{5+x}Sb_5P_{2-x}Si_xO_{20}$ in order to improve the ionic conductivity by increasing the K^+ concentration. However, only multiphase products formed. Next we focused on substitution for the antimony site.

Isoelectronic substitution was carried out on $K_5Sb_5P_2O_{20}$ by replacing some of the Sb^{5+} (0.74 Å) with the larger Nb^{5+} (0.78 Å) and Ta^{5+} (0.78 Å) ions and also with the smaller V^{5+} (0.68 Å) ion. Our objective here was 2-fold: First, to study the effect of changes in the bottleneck size on ionic conductivity—one expects the ionic conductivity to increase with enlargement in the bottleneck size when Sb^{5+} is replaced by Nb^{5+}/Ta^{5+} and to decrease with V^{5+} substituting for Sb^{5+}. Second, to study the effect of substitutions on the K^+–oxygen bond strength and how that affects the ionic conductivity. Since Sb is more electro-

(11) Kummer, J. T. *Prog. Solid State Chem.* **1972**, *7*, 141.

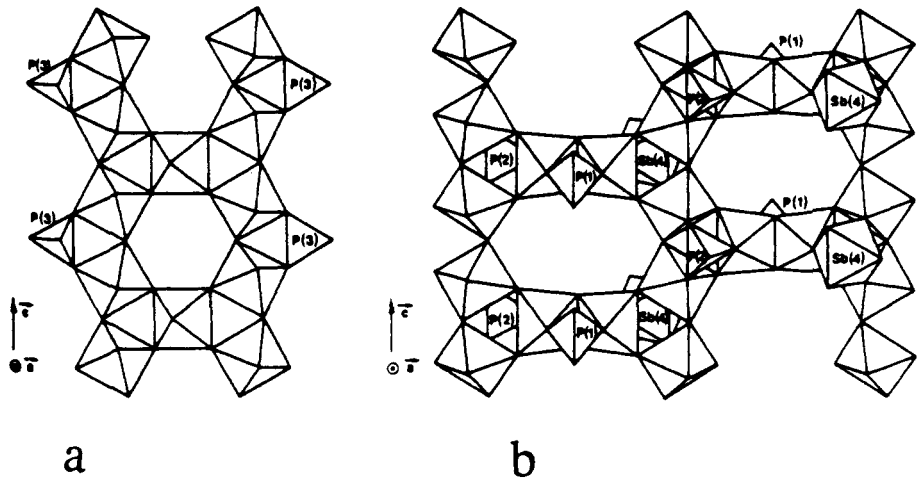

Figure 5. [100] view of $K_5Sb_5P_2O_{20}$ structure showing (a) the ringlike feature (indicated by hatched octahedra) and (b) the edge-sharing along *b*.

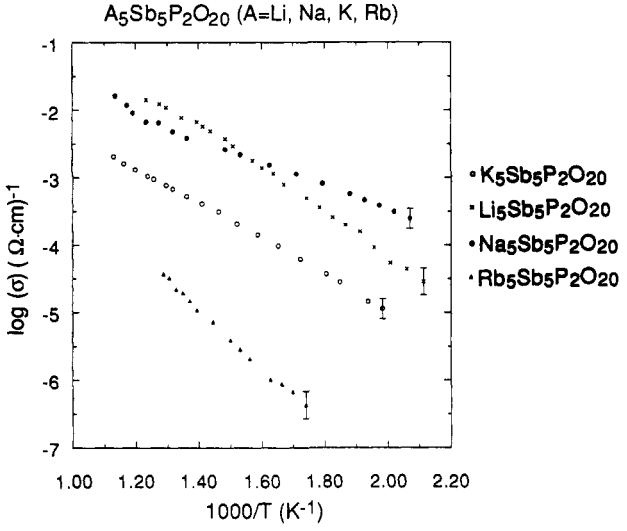

Figure 6. Temperature dependence of the ionic conductivity of $A_5Sb_5P_2O_{20}$ (A = Li, Na, K, Rb).

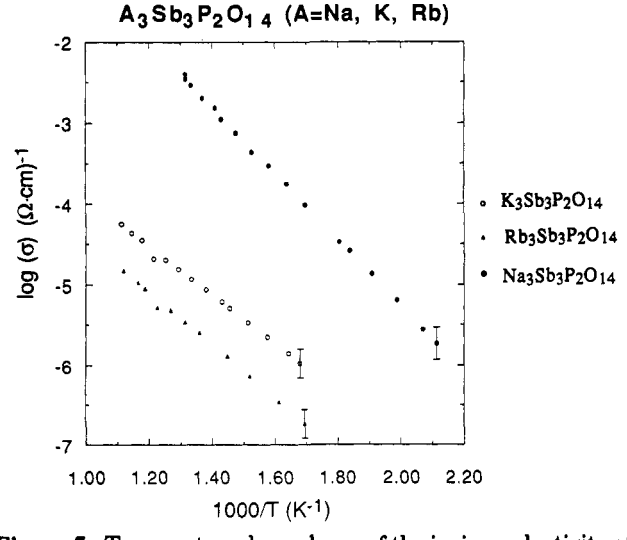

Figure 7. Temperature dependence of the ionic conductivity of $A_3Sb_3P_2O_{14}$ (A = Na, K, Rb).

negative than V, Nb, or Ta (Table II), one expects the Sb–O bond to be more covalent (less ionic) than the V–O, Nb–O, or Ta–O bonds. Consequently, the K^+–oxygen bond in K–O–V, K–O–Nb, and K–O–Ta should be stronger than the K^+–oxygen bond in K–O–Sb. Thus, the electronegativity factor is expected to decrease the ionic conductivity in substituted $K_5Sb_{5-x}M_xP_2O_{20}$ (M = V, Nb, Ta) as x increases. Similar findings were reported by Riviere et al.[12] on the proton conductivity of the cubic pyrochlores $H_{2x}Sb_{2x}W_{2-2x}O_6{\cdot}nH_2O$ when Sb^{5+} was replaced by the less electronegative W^{6+}.

Partial substitution of Sb by V, Nb, or Ta was observed. However, the limit of substitution decreases from Ta (x = 3) to Nb (x = 2) to V (x = 1) in $K_5Sb_{5-x}M_xP_2O_{20}$ (M = V, Nb, Ta). It appears that the 3D structure forms preferably with the larger cations. Moreover, $K_5Sb_4VP_2O_{20}$ is light yellow; the color intensified upon heating to higher temperature, which could be indicative of mixed valency, V^{4+}/V^{5+}, of the vanadium. Further evidence of electronic conduction in the V-substituted phase was seen in the Cole–Cole plot of the ac impedance spectrum, which showed only a resistive component indicative of electronic (not ionic) conductivity. Therefore, no further characterization of $K_5Sb_4VP_2O_{20}$ was carried out, since meaningful comparison with Nb- or Ta-substituted KPAs could not be made.

In the $K_5Sb_{5-x}M_xP_2O_{20}$ (M = Nb, Ta) series, the limit of substitution (x) is two and three for Nb and Ta respectively. The unit-cell parameters increase with x (Figure 8). Moreover, the increase of lattice parameters along *b* or *c* is not restrained by the edge-sharing or the "ringlike" feature respectively (as was in the case of the ion-exchanged compounds) since the increase of unit-cell parameters seen in the partially substituted compounds is caused by an expansion of the lattice framework and not by an expansion of the cavity (as a result of small cations ion-exchanged by large cations). It is also interesting to note that the $K_5Sb_{5-x}Ta_xP_2O_{20}$ series has larger lattice parameters than the $K_5Sb_{5-x}Nb_xP_2O_{20}$ series, which is consistent with the slightly larger size of Ta^{5+} relative to Nb^{5+} (even though both were reported to be the same size[13]).

Figure 9 shows the temperature dependence of ionic conductivity of the $K_5Sb_{5-x}Nb_xP_2O_{20}$ and $K_5Sb_{5-x}Ta_xP_2O_{20}$ series. In both systems, the ionic conductivity increases significantly with increasing x, so that the ionic conductivity of $K_5Sb_3Nb_2P_2O_{20}$ almost equals that of $Na_5Sb_5P_2O_{20}$. The increase in the ionic conductivity of the sub-

(12) Riviere, M.; Fourquet, J. L.; Grins, J. Nygren, M. *Mater. Res. Bull.* **1988**, *23*, 965.
(13) Shannon, R. D. *Acta Crystallogr.* **1976**, *A32*, 751.
(14) Pauling, L. *The Nature of the Chemical Bond*, 3rd. ed.; Cornell University Press: Ithaca, NY, 1960; Chapters 13–16.

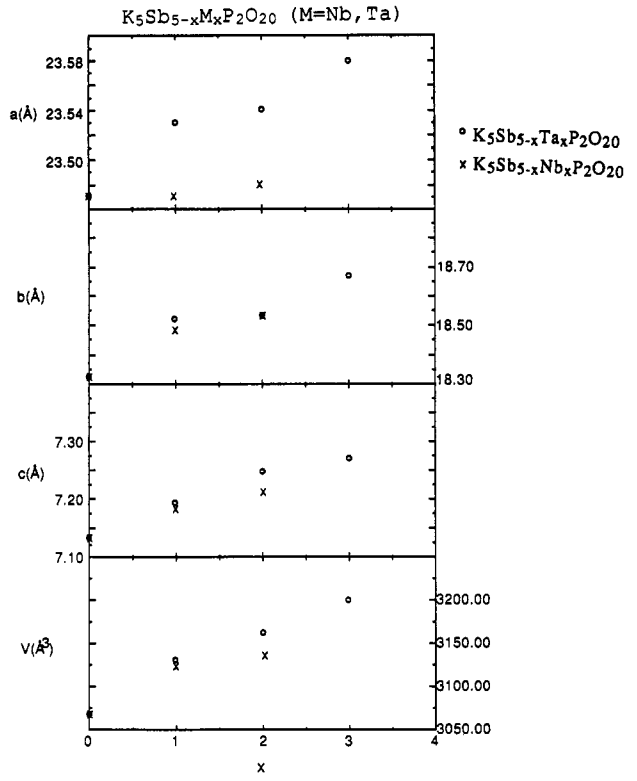

Figure 8. Variation of the unit-cell parameters as a function of x in $K_5Sb_{5-x}M_xP_2O_{20}$ (M = Nb, Ta). The errors in a, b, c, and V are 0.01 Å, 0.02 Å, 0.005 Å, and 2.5 Å^3, respectively.

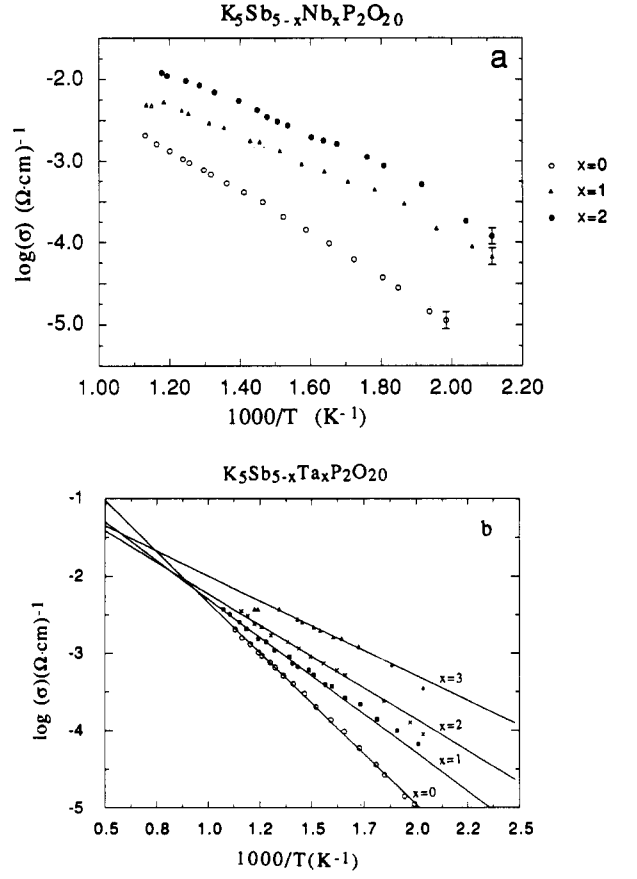

Figure 9. Temperature dependence of the ionic conductivities of (a) $K_5Sb_{5-x}Nb_xP_2O_{20}$ and (b) $K_5Sb_{5-x}Ta_xP_2O_{20}$. The errors are the same in both a and b.

stituted samples is ascribed to the increase in the bottleneck size, as evidenced by the increase in the unit-cell parameters with increasing x (Figure 8). The location of

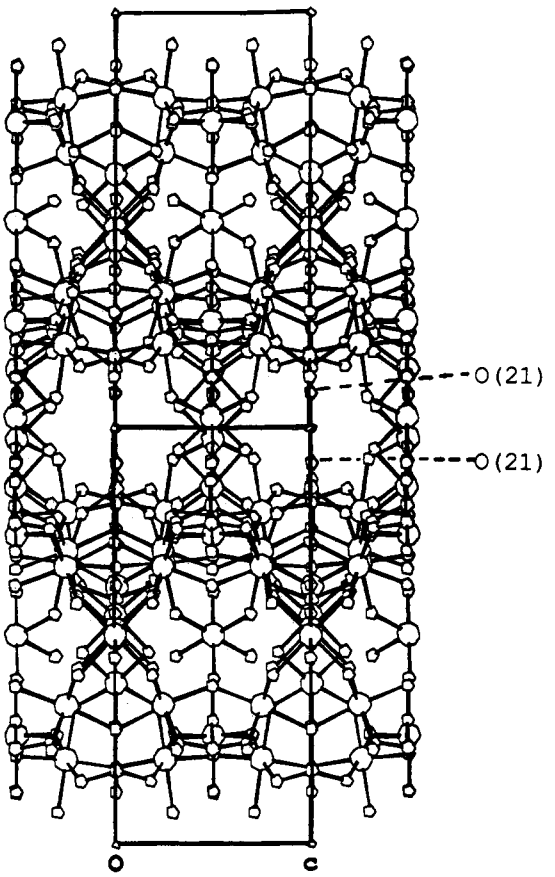

Figure 10. [110] view of the structure of ($Sb_5P_2O_{20}^{5-}$) framework. The O(21)–O(21) distance indicates the possible bottleneck.

the bottleneck site is further clarified when one views the structure in the [110] plane (Figure 10). The narrowest region (i.e., bottleneck) was calculated to be ~4.1 Å between two O(21) atoms; the K(9) ion is located between these oxygens in the least-occupied potassium site (i.e., the occupancy factor is the lowest). Thus, the observed increase in the ionic conductivity probably resulted from an expansion of the O(21)–O(21) distance.

Upon further examination of Figure 9b, one notes that the temperature-dependent ionic conductivities of the $K_5Sb_{5-x}Ta_xP_2O_{20}$ series almost converge to one point at high temperature. The activation energies decrease with increasing amount of tantalum substituted for antimony (Table I); this indicates that in the $K_5Sb_{5-x}Ta_xP_2O_{20}$ series, the potassium mobility is the same (i.e., same preexponential term) and the gradual expansion of the bottleneck (consistent with the decreasing E_a's observed) is the dominant factor for the observed increase in the ionic conductivity. No correlation in E_a's (Table I) can be made for the $K_5Sb_{5-x}Nb_xP_2O_{20}$ series due to the low limit of solubility (x_{max} = 2); nevertheless, the E_a's of the substituted phases are significantly lower than that of the unsubstituted phase. This is consistent with a larger bottleneck in the substituted materials.

In an attempt to increase the ionic conductivity of $K_5Sb_3Nb_2P_2O_{20}$, which has the highest observed ionic conductivity of all the KPA samples, ion-exchange reactions were carried out to replace potassium by sodium (e.g., sodium-exchanged $K_5Sb_5P_2O_{20}$ has higher conductivity than that of the host material). Surprisingly, the ionic conductivity of the sodium-exchanged sample, $Na_5Sb_3Nb_2P_2O_{20}$, did not exceed that of $Na_5Sb_5P_2O_{20}$. In fact, the highest conducting sample was obtained from the room-temperature reaction between $H_5Sb_3Nb_2P_2O_{20}\cdot xH_2O$ and 0.1 M NaOH. This reaction at higher temperature or the

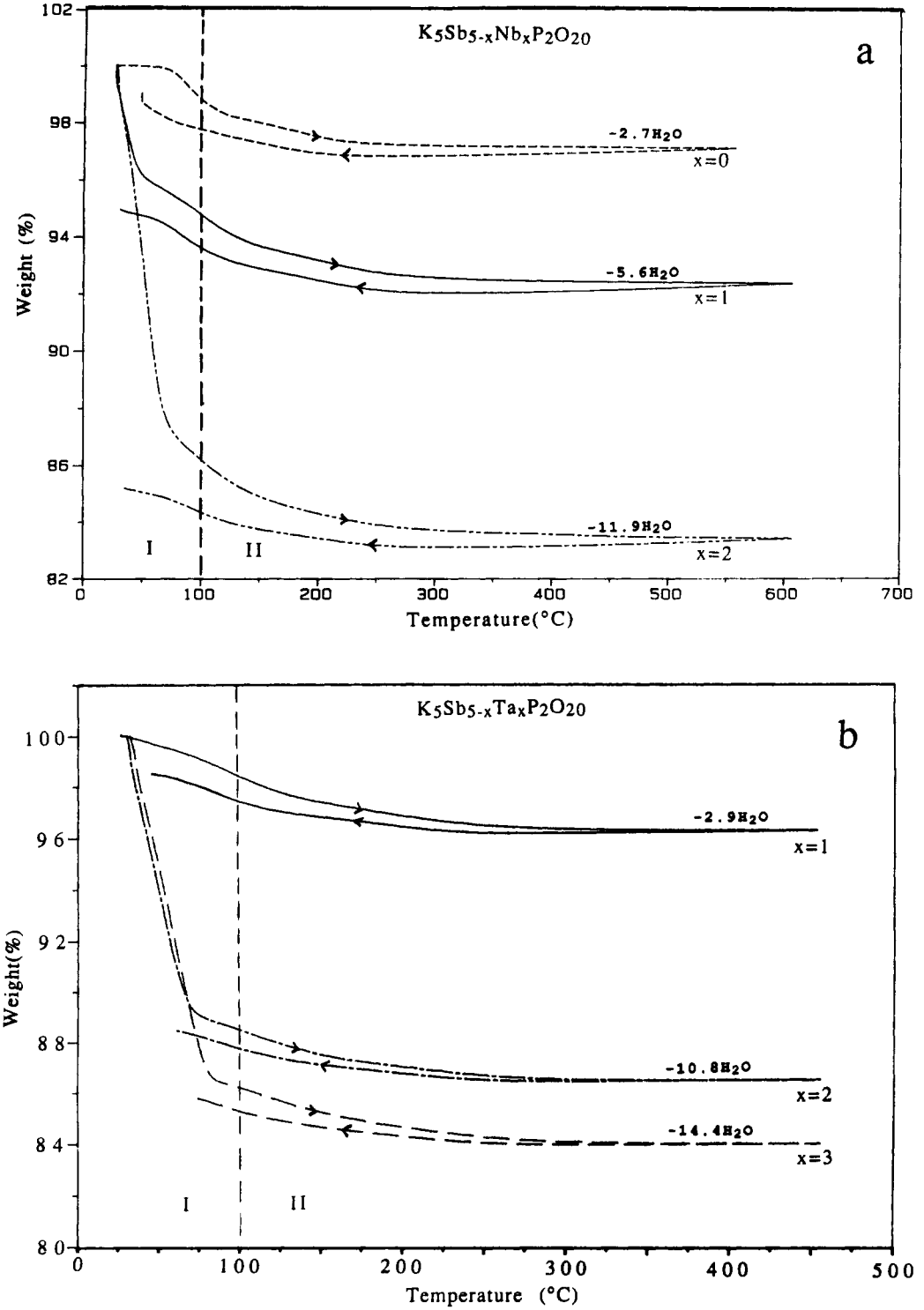

Figure 11. TGA curves of (a) $K_5Sb_{5-x}Nb_xP_2O_{20}\cdot xH_2O$ and (b) $K_5Sb_{5-x}Ta_xP_2O_{20}\cdot xH_2O$ compounds.

hydrothermal synthesis of 1 M $NaNO_3$ and $K_5Sb_3Nb_2P_2O_{20}$ always resulted in sodium-exchanged samples with lower ionic conductivities. Moreover, none of the sodium-exchanged $K_5Sb_3Nb_2P_2O_{20}$ shows a reversible TGA curve, as was seen also in $Na_5Sb_5P_2O_{20}\cdot xH_2O$ (Figure 2). Thus, there is always some decomposition accompanying the ion-exchange with sodium in the substituted sample, as evidenced by the poor crystallinity of the ion-exchanged samples when the ion-exchange reaction is carried out at elevated temperature. These results suggest that K^+ is bonded more tightly to the ($Sb_3Nb_2P_2O_{20}^{5-}$) than to the ($Sb_5P_2O_{20}^{5-}$) framework. This could be ascribed to the lower electronegativity in the Nb/Ta than in the Sb compound (Table II), which results in a stronger K–O bond in $K_5Sb_{5-x}M_xP_2O_{20}$ than in $K_5Sb_5P_2O_{20}$ as described above.

The ion-exchange results of the partially substituted phosphatoantimonates, coupled with the fact that $K_5Sb_2Ta_3P_2O_{20}$ has a lower ionic conductivity than $K_5Sb_3Nb_2P_2O_{20}$ despite the larger bottleneck of the former, indicate that the bottleneck is optimal for $K_5Sb_3Nb_2P_2O_{20}$, too large for $K_5Sb_3Ta_2P_2O_{20}$, and not quite large enough for $K_5Sb_5P_2O_{20}$. In $Na_5Sb_{5-x}M_xP_2O_{20}$ it is not possible to conclude how the bottleneck affects the ionic conductivity because of the instability of the structure.

TGA measurements were carried out to determine the effects of substitution on hydration. Prior to measurement,

the samples were equilibrated in a closed container over water, at room temperature overnight, in an attempt to attain the maximum amount of hydrate water. In contrast to $K_5Sb_5P_2O_{20}$, two distinctive regions can be seen in the TGA curves of the substituted samples (Figure 11). The majority of water is lost below 100 °C in the substituted samples. Above ~100 °C, the amount of water lost is almost identical in both the substituted and $K_5Sb_5P_2O_{20}$ samples (Figure 11). The two regions in the TGA curves of the substituted samples (i.e., I and II) are attributed to two types of water: surface and lattice water; $K_5Sb_5P_2O_{20}$ has only lattice water. The adsorption of surface water in the substituted samples could be due to their smaller particle size (hence larger surface area) compared with that of $K_5Sb_5P_2O_{20}$. Alternatively, the substitution of Nb/Ta for the more electronegative Sb (Table II) is expected to increase the formal charge on the lattice oxygen in $K_5Sb_{5-x}M_xP_2O_{20}$, which results in a more hygroscopic sample.

Acknowledgment. We thank Prof. Piffard of Universite de Nantes for helpful discussions and providing the structural figures for publication. This work was supported by the Office of Naval Research.

New Class of Electron Acceptors Having High Polymer Dispersibility, Unsymmetrically Substituted Diphenoquinones, and Their Application as Electron Transport Materials

Yasuhiro Yamaguchi and Masaaki Yokoyama*

Chemical Process Engineering, Faculty of Engineering, Osaka University, Yamadaoka, Suita, Osaka 565, Japan

Received April 1, 1991. Revised Manuscript Received May 13, 1991

A new class of electron acceptors, unsymmetrically substituted diphenoquinones with methyl and bulky alkyl substituents, has been developed for electron-transport compounds, which possess high dispersibility in a wide range of polymers owing to their unsymmetrical and bulky substitutions. 3,5-Dimethyl-3′,5′-di-*tert*-butyl-4,4′-diphenoquinone (MBDQ), a representative member of these acceptors, dispersed molecularly in polycarbonate exhibited electron mobilities over 10^{-6} cm^2/V s at a conventional concentration of 40 wt %, which are the highest for electron transport in molecularly doped polymers. The photoinduced discharge measurements demonstrated that electrons can be injected from titanylphthalocyanine into the MBDQ-doped polycarbonate, indicating a possible application to xerography.

Introduction

Charge-transport phenomena in molecularly doped polymers (MDPs) have attracted considerable attention because of their technological importance as charge-transport materials for organic photoreceptors in xerography.[1] These materials are also of interest for the basic understanding of charge transfer in amorphous organic solids. Usually, these are supplied as binary solid solutions that are comprised of a transport-active molecule and a film-forming polymeric binder. From the chemical point of view, charge transport in such MDPs is an electric-field-driven chain of redox processes between neutral molecules and the corresponding radical ions, i.e., cation and anion radicals for positive (hole) and negative (electron) charge transport, respectively.[2-4] It is, therefore, required that the molecules for hole and electron transport should be electron-donating and electron-accepting in their ground states, respectively.

A large number of hole-transporting electron donors have emerged so far, and many of them, such as arylamine and hydrazone derivatives, have been widely used in practical xerographic photoreceptors. The hole transport in MDPs, therefore, has been extensively investigated.[2-17] The hole mobilities are largely in the range 10^{-4}–10^{-6} cm^2/V s and increase with an increase in dopant concentration. In most cases, the mobilities are thermally activated with a field-dependent activation energy that may be also temperature-dependent.[7,9,11,14,15,21e]

In contrast to the abundance of hole-transport materials, only a few electron acceptors have been reported as elec-

(1) Schein, L. B. *Electrophotography and Development Physics*; Springer: New York, 1988.
(2) Mort, J.; Pfister, G.; Grammatica, S. *Solid State Commun.* **1976**, *18*, 693.
(3) Stolka, M.; Yanus, J. F.; Pai, D. M. *J. Phys. Chem.* **1984**, *88*, 4707.
(4) Facci, J. S.; Stolka, M. *Philos. Mag. B* **1986**, *54*, 1.
(5) Pfister, G. *Phys. Rev. B* **1977**, *16*, 3676.
(6) Borsenberger, P. M.; Mey, W.; Chowdry, A. *J. Appl. Phys.* **1978**, *49*, 273.
(7) Bässler, H.; Schönherr, G.; Abkowitz, M.; Pai, D. M. *Phys. Rev. B* **1982**, *26*, 3105.
(8) Pai, D. M.; Yanus, J. F.; Stolka, M.; Renfer, D. S.; Limburg, W. W. *Philos. Mag. B* **1983**, *48*, 505.
(9) Bässler, H. *Philos. Mag. B* **1984**, *50*, 347.
(10) Santos Lemus, S. J.; Hirsh, J. *Philos. Mag. B* **1986**, *53*, 25.
(11) Schein, L. B.; Rosenberg, A.; Rice, S. L. *J. Appl. Phys.* **1986**, *60*, 4287.
(12) Mack, J. X.; Schein, L. B.; Peled, A. *Phys. Rev. B* **1989**, *39*, 7500.
(13) Schein, L. B.; Glatz, D.; Scott, J. C. *Phys. Rev. Lett.* **1990**, *65*, 472.
(14) Borsenberger, P. M. *J. Appl. Phys.* **1990**, *68*, 5682.
(15) Borsenberger, P. M. *J. Appl. Phys.* **1990**, *68*, 6263.
(16) Tanaka, H.; Yamaguchi, Y.; Yokoyama, M. *Denshi Shashin Gakkaishi* **1990**, *29*, 366.
(17) Yuh, H.-J.; Pai, D. M. *Mol. Cryst. Liq. Cryst.* **1990**, *183*, 217.

0897-4756/91/2803-0709$02.50/0